Malaysian Journal of Chemistry, 2020, Vol. 22 (1), 33-46
(Special Issue: *7th International Conference for Young Chemists - ICYC 2019*, Universiti Sains Malaysia)

Adsorption Kinetics for Carbon dioxide Capture using Bismuth(III) Oxide Impregnated on Activated Carbon†

Azizul Hakim Lahuri[1*], Rohana Adnan[2], Mohd. Hafiy Mansor[2], Nur Farah Waheed Tajudeen[2], and Norazzizi Nordin[2]

[1]Department of Basic Science and Engineering, Faculty of Agriculture and Food Sciences, Universiti Putra Malaysia - Bintulu Campus, P. O. Box 396, Nyabau Road, 97008 Bintulu, Sarawak, Malaysia
[2]School of Chemical Sciences, Universiti Sains Malaysia, 11800 USM, Pulau Pinang, Malaysia
*Corresponding author (e-mail: azizulhakim@upm.edu.my)

Bismuth(III) oxide (Bi_2O_3)-impregnated activated carbon (AC) composites were synthesized and prepared at different Bi_2O_3 loading. Adsorption capacities of the adsorbents were determined at varying adsorption temperatures by using thermogravimetric analysis (TGA). CO_2 regeneration was successfully performed at 400°C, indicating the adsorbents were feasible with CO_2 adsorption and desorption processed. 0.1Bi/AC was shown as the most efficient adsorbent at optimum adsorption temperature of 30°C with CO_2 adsorption capacity of 58.71 mg CO_2/g adsorbent. Although the BET surface area of 0.1Bi/AC was reduced (783.25 m^2/g) compared to AC only, the Bi_2O_3 loading noticeably enhanced CO_2 chemisorption due to the affinity to attract CO_2. The adsorption kinetics indicated that chemisorption dominated the adsorption process as the data fitted well in the pseudo-second-order kinetic model. The stability of CO_2 capture capacity was consistent over 5 cycles, with slightly higher than AC only, ascribed to the chemical adsorption by interactions of carbonate species with Bi_2O_3 besides the physisorption on AC. These features exhibited a potential for large scale applications of the adsorbent, which favored ambient conditions for CO_2 adsorption and feasible desorption process.

Key words: CO_2 capture; adsorption kinetics; activated carbon; bismuth(III) oxide

Received: September 2019; Accepted: December 2019

Global warming is widely ascribed to an increase in the atmospheric levels of greenhouse gases [1]. According to the Intergovernmental Panel on Climate Change, the major greenhouse gas emissions in 2017 were carbon dioxide (CO_2), methane (CH_4), nitrogen oxide (NO), and fluorinated gases [2]. However, among all of the gases, the main contribution to the present global warming trend is about 81% by CO_2 emission and it gives the largest impact on climate change [3,4]. The recent global concentration of CO_2 in the atmosphere was 408.72 ppm in May 2018 but rose to 411.35 ppm in May 2019. Current CO_2 level is higher than the CO_2 atmospheric safety limit of 350 ppm since the 1980's [5, 6]. The vast amount of CO_2 is emitted through the burning of fossil fuels, such as petroleum, coal, oil, and gas; as well as releasing other pollutants [1]. The density of CO_2 is about 50% higher than that of dry air, thus is able to trap heat in the atmospheric level. In addition, human activities such as development, uncontrolled forest burning, and deforestation [7] accelerate CO_2 emissions well beyond it natural levels. The awareness on carbon dioxide emissions has led to increase in efforts to reduce its environmental impact, including preventive and remediation methods.

Innovative CO_2 capturing technologies are needed in order to overcome the excess of CO_2 in the including chemical absorption [2], physical adsorption [8], membrane separation [9], liquid amine absorption [10], and the use of solid adsorbents [11] and selective membrane [12]. Among all of these techniques, adsorption has been considered as one of the most promising techniques in commercial and industrial applications because of the low energy requirement, cost advantage, and ease of applicability over a relatively wide range of temperature and pressure [13]. Adsorption on solid adsorbents can take place via physisorption and chemisorption. Physisorption requires low heat as it only involves intermolecular forces such as van der Waals forces, hydrogen bonds, and electrostatic forces. For chemisorption, the substance normally binds to a certain site on the adsorbent, which leads to higher heat of adsorption process. Meanwhile, CO_2 regeneration is another process which not all works reported, and it is important to utilize CO_2 by converting it to precious materials such as fuel.

Activated carbon (AC) has been widely used as support for CO_2 capture because of its favorable properties for gas sorption due to the wide availability, low cost, high thermal stability and low sensitivity to moisture, large surface area, and distinct properties that lead to high adsorption capacities [3,6]. Furthermore, it possesses moderate strengths of

†Paper presented at the 7th International Conference for Young Chemists (ICYC 2019), 14-16 August 2019, Universiti Sains Malaysia.

adsorption for gases that ease the desorption process, resulting in robustness in cyclic operations [14]. Modifications of AC surfaces loaded with different metal oxides have been reported to facilitate improvement especially in chemisorption [6]. Studies of calcium oxide (CaO), which was among the earliest materials used as adsorbent in CO_2 adsorption, included kinetics, regeneration by desorption with thermal exposure, and adsorption capacity [20]. Numerous metal oxides, such as lanthanum sesquioxide (La_2O_3), silver oxide (AgO), titanium oxide (TiO_2), copper oxides (CuO and Cu_2O), nickel oxide (NiO), titanium dioxide (TiO_2), iron oxides (FeO, Fe_2O_3, and Fe_3O_4), strontium oxide (SrO), and cerium oxide (CeO_2), were studied for their CO_2 adsorption capacity [14-22].

Studies of bismuth(III) oxide (Bi_2O_3), which is a remarkable photocatalyst for dye removal [23-25], have reported to exhibit potential effective degradation. Its catalytic activity in NO and hydrocarbon reduction also showed progressive results [26]. Although the activity of Bi_2O_3 for CO_2 adsorption was reported by Luevano-Hipolito [27], however, it was not included subsequently with CO_2 regeneration. Thus, in this work, Bi_2O_3 was used to impregnate AC to study the CO_2 capture capability, the CO_2 capture recyclability, and determine the adsorption kinetics.

METHODOLOGY

Adsorbent Preparation

Activated carbon (AC) and bismuth nitrate pentahydrate ($Bi(NO_3)_3.5H_2O$) were obtained from R&M Chemicals, Essex (UK) and QReC, respectively. Meanwhile, sodium bicarbonate ($NaHCO_3$) was purchased from Acros Organics (USA). All chemicals used in this research were of analytical grade. They were used without any further modification and purification. The adsorbent was synthesized by using the method reported by Shah et al. [28], with slight modifications. A solution of 0.05 M $Bi(NO_3)_3.5H_2O$ was mixed with 5 g of AC by stirring with a magnetic stirrer at 200 rpm up to 8 hr to ensure homogeneous mixing. Then, the mixture was filtered and washed with 600 mL of 1% sodium bicarbonate solution, $NaHCO_3$. The residue was soaked overnight in 400 mL of 1% $NaHCO_3$ solution. The mixture was decanted and the residue was washed again with 400 mL of distilled water. Next, the residue was air-dried for 2 hours and then heated in an oven for 6 hours at 110℃. Similarly, 0.1 and 0.5 M absorbents were also prepared. The adsorbents were labelled as *x*Bi/AC where *x* was the molarities of 0.05, 0.1, and 0.5.

Characterization

The thermal stability of the adsorbents was characterized by thermogravimetric analysis (TGA) using Perkin Elmer STA 6000. Approximately 10 mg of the samples were subjected to heating until 900°C at the rate of 30°C/min and under N_2 atmosphere with a flow rate of 20 mL/min. The crystallinity of the adsorbents was determined by X-ray diffraction (XRD) using Bruker AXS D8 to observe the crystalline phase. The 2θ diffraction was recorded from 10° to 90° to verify the crystal structure. The crystalline phase interpretation was done by matching the X-ray diffractograms with standard diffraction data (JCPDS). Carl Zeiss Leo Supra 50VP Field Emission scanning electron microscope (SEM) equipped with Oxford INCA-X energy dispersive microanalysis system (EDX) was used to observe the surface morphology and the elemental composition of AC and Bi/AC. Nitrogen (N_2) adsorption-desorption isotherm was used to determine the surface properties of the composites using gas sorption analyzer ASAP 2020. The analysis was recorded at 77 K and in relative pressure (P/Po) ranging from 0 to 1.0. The infrared (IR) spectra were obtained by Fourier Transform Infrared (FTIR) spectroscopy on Perkin Elmer 2000 using the KBr disc method. The spectra were recorded between 4000 and 400 cm^{-1}.

CO_2 Capture Studies

TGA was used to study the CO_2 adsorption capacity through the weight change of the adsorbent. Approximately 10 mg of adsorbent was placed in a sample cell and heated from 30 to 350°C. The adsorbent was held at 350°C for 30 minutes for the purpose of the cleaning process to eliminate humidity and moisture by flowing N_2 gas. It was then cooled to 30°C and saturation CO_2 adsorption was conducted by introducing 99.98% of CO_2 adsorbate for 20 minutes. After adsorption, the gas was switched to N_2 gas to perform the desorption at 30 to 900°C. CO_2 capture reaction process was conducted at a temperature rate of 30°C/min with a gas flow rate of 20 mL/min. The effect of adsorption temperature at 30, 40, and 50°C was investigated to optimize the adsorption capacity. The optimum adsorption temperature was used in cyclical CO_2 capture to evaluate the stability of the composites.

Adsorption Kinetics Modelling

The adsorption data for the effect of adsorption temperature were examined by fitting with pseudo-first-order and pseudo-second-order kinetic models. The adsorption kinetic parameters and R^2 values were used to determine the best-fitted model. This analysis provided insights into understanding the adsorption dynamics and its performances.

RESULTS AND DISCUSSION

Adsorbents Characterization

Thermal stability of the adsorbents was used to obtain information about stability toward thermal exposure due to the necessity during the desorption process. Figure 1 shows the thermal stability curves of the

adsorbents exhibit initial steep weight loss until 110°C, which corresponds to the loss of moisture from the adsorbents. In this process, AC and 0.1Bi/AC lost around 12% and 18.7% in initial weight, respectively. Gradual weight loss observed until 450°C may be due to trapped humidity gases. It is noteworthy to observe 0.1Bi/AC exhibited weight lost around 3.84% in the region of 450 to 600°C, which ascribed from the removal of oxygen. The formula unit changed from Bi_2O_3 to $Bi_2O_{2.902}$ upon heating until 600°C [29]. Both adsorbents were observed not to experienced distinct weight loss above 600°C, thus showed that no other weight loss occurred.

XRD diffractograms of AC and 0.1Bi/AC are shown in Figure 2. Typical amorphous peaks for AC were observed at 23.1° and 42.8°. The amorphous peaks intensity decreased after loading with Bi_2O_3 and 0.1Bi/AC was transformed into a crystalline structure. It showed planes (201), (220), (002), (222), (400), (203), and (421) corresponded to α-Bi_2O_3 (JCPDS, No. 05-0519). Meanwhile, planes (002), (011), (004), and (114) could be indexed to a non-toxic and environmentally friendly compound of $(BiO)_2CO_3$ (JCPDS, No. 41-1488) with tetragonal structure. The exposure of the adsorbent to ambient CO_2 resulted in carbonate (CO_3^{2-}) formation as $(BiO)_2CO_3$. Thus, it is important to perform the cleaning process by heating the adsorbent to remove undesirable CO_3^{2-} prior to evaluating CO_2 adsorption capacity.

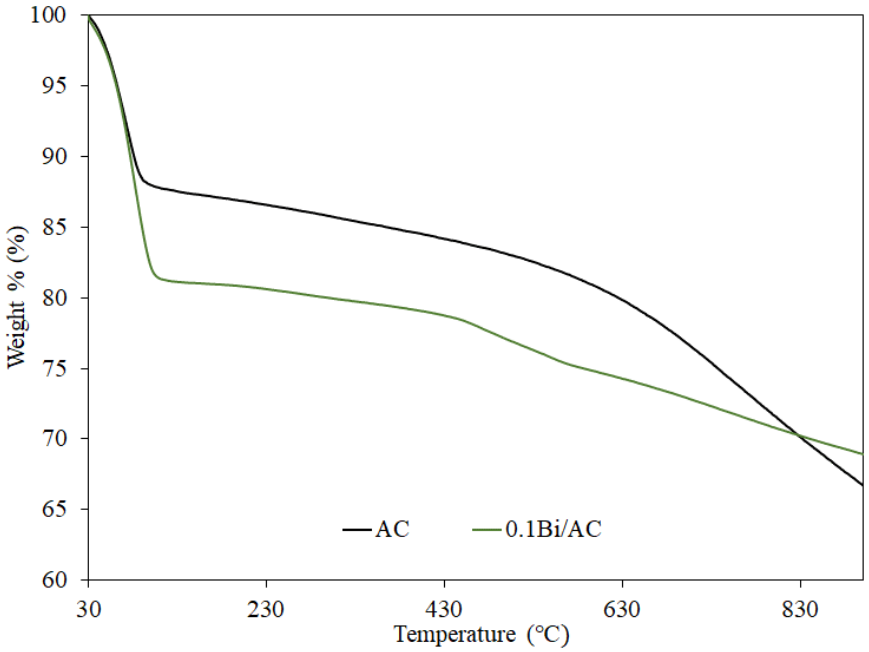

Figure 1. Thermal stability of adsorbents

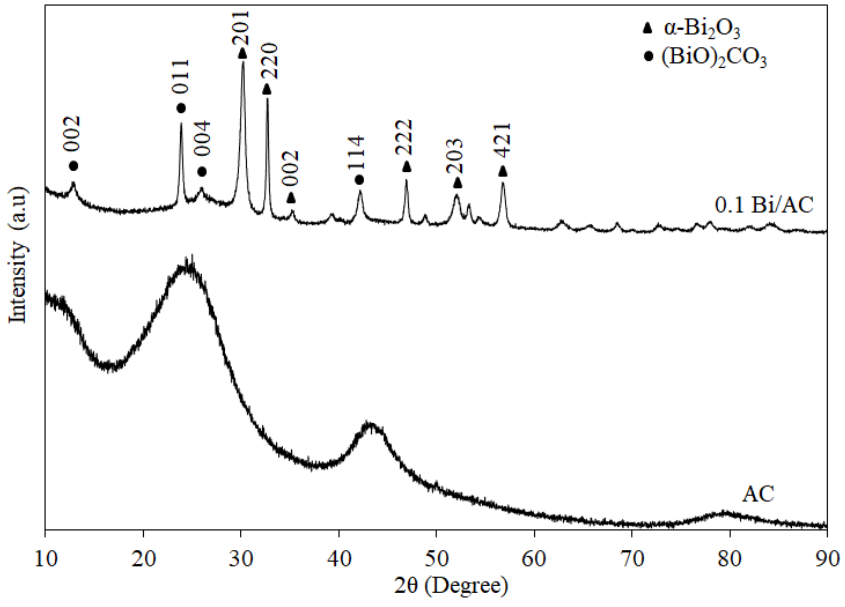

Figure 2. XRD patterns of AC and 0.1Bi/AC

The surface morphology of the adsorbents was observed through SEM images as shown in Figure 3. AC surfaces had an irregular porous structure in nature. Meanwhile, the surfaces of 0.1Bi/AC and 0.5Bi/AC were rougher and non-uniform that gave high heterogeneity surface. The stirring time during synthesis confirmed that Bi_2O_3 was successfully impregnated on AC with Bi_2O_3 particles well dispersed on AC. A high concentration of Bi_2O_3 loading for 0.5Bi/AC caused excessive crystal growth that led to particle agglomeration and gave rise to crystalline structures on AC surfaces. The detailed elemental compositions of the adsorbent were identified from EDX results. The EDX spectra of all the adsorbents contained C and O. Whereas 0.1Bi/AC and 0.5Bi/AC contained C, O, and Bi. The percentage of oxygen increased upon Bi_2O_3 loading on AC. High surface coverage of Bi_2O_3 particles on AC for 0.5Bi/AC resulted in low C presence on the surface.

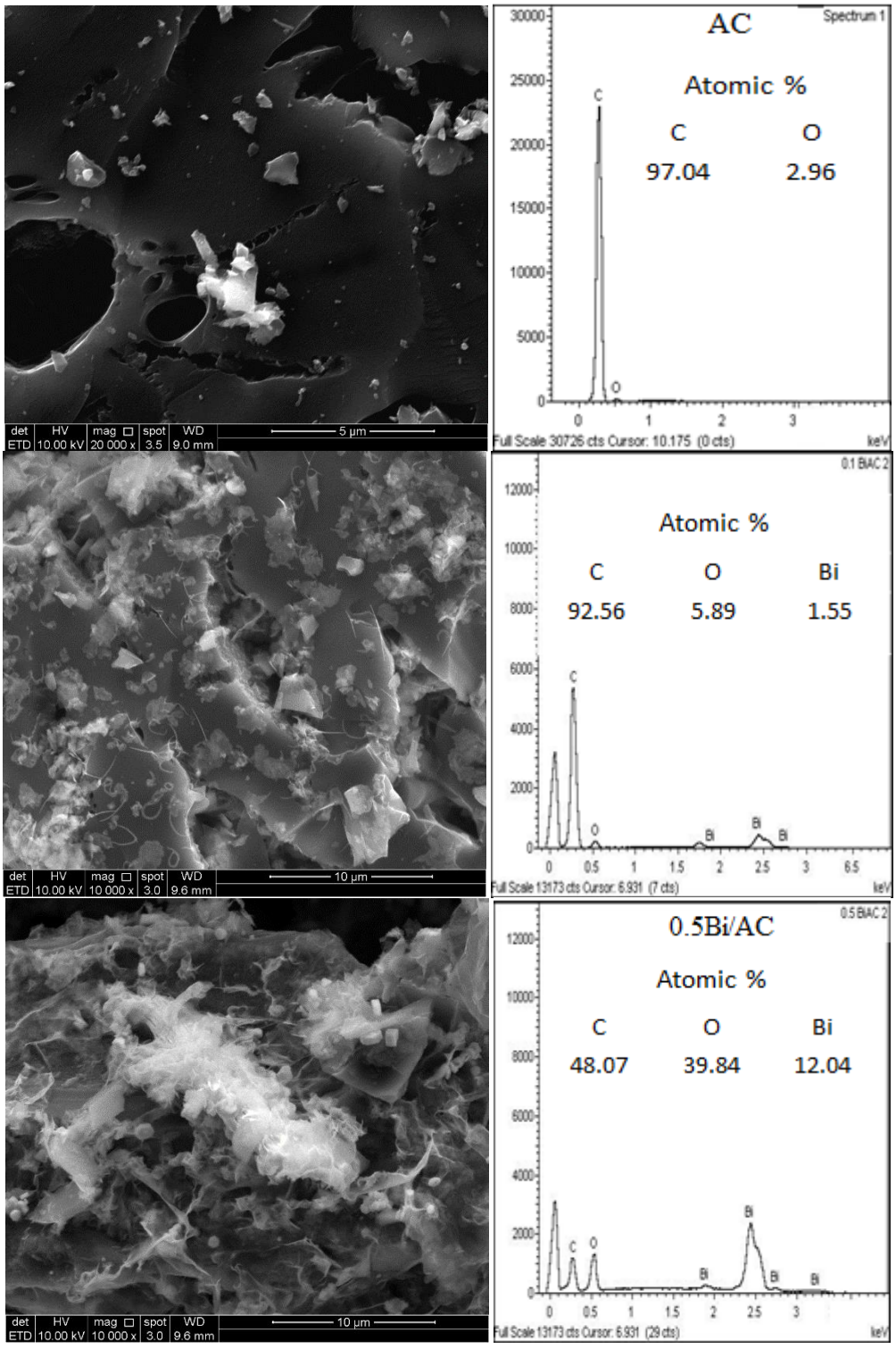

Figure 3. SEM micrographs and EDX spectra of adsorbents

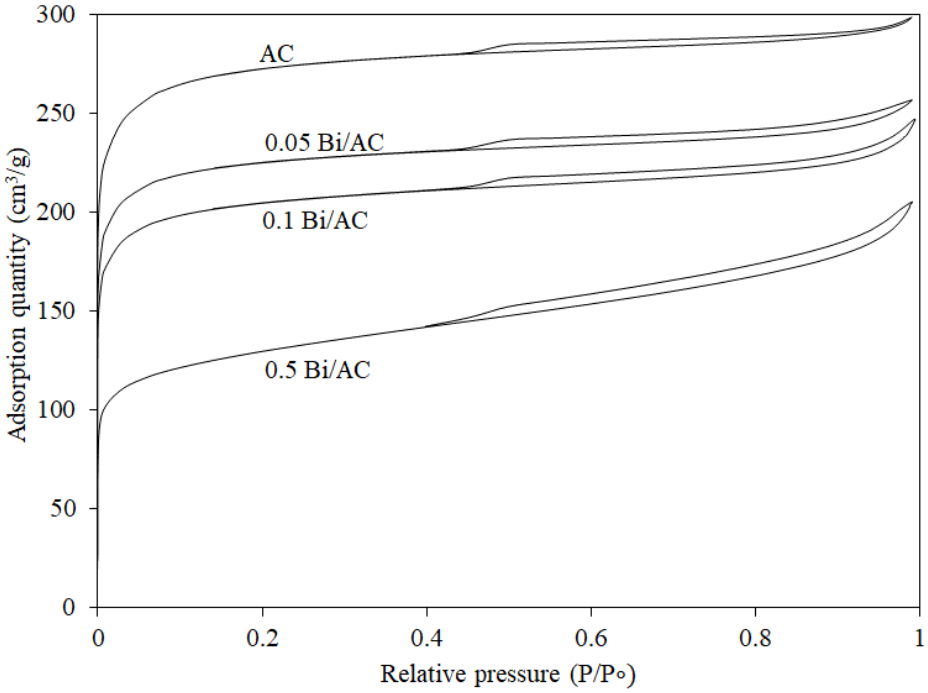

Figure 4. N_2 adsorption-desorption isotherms

Table 1. Textural properties of adsorbents

Sample	BET surface area, S_{BET}(m^2/g)	Mesopore surface area, S_{meso} (m^2/g)	Micropore surface area, S_{mic} (m^2/g)	Total pore volume, V_{tot} (cm^3/g)	Micropore volume, V_{mic} (cm^3/g)	Average pore diameter (nm)
AC	1043.59	170.99	872.61	0.46	0.35	1.76
0.05Bi/AC	863.93	130.16	733.78	0.39	0.29	1.82
0.1Bi/AC	783.25	134.60	648.65	0.37	0.26	1.89
0.5Bi/AC	478.08	181.78	296.31	0.31	0.12	2.59

N_2 adsorption-desorption isotherms and the textural properties are described in Figure 4 and Table 1, respectively. The adsorbents exhibited Type I isotherm and possessed H4 hysteresis according to IUPAC classification [30, 31]. The initially steep region was due to strong adsorption on typical microporous materials and H4 hysteresis showed the adsorbents possessed narrow slit-shaped pores of mesopores. The hysteresis for 0.5Bi/AC had the largest area compared to the rest of the adsorbents attributed to Bi_2O_3 particles on AC surfaces creating their own mesopore structure. The specific Brunauer-Emmett-Teller (BET) surface area (S_{BET}) and total pore volume (V_{tot}) decreased with high Bi_2O_3 loading on AC. S_{BET} for 0.5Bi/AC substantially decreased (478.08 m^2/g) compared to AC (1043.59 m^2/g), which anticipated lower adsorption sites. Similarly, the micropore surface area (S_{mic}), evaluated from the t-plot method, showed the same trend as S_{BET}. Nonetheless, the mesopore surface area (S_{meso}), also evaluated from the t-plot method, was significantly high (181.78 m^2/g), especially for 0.5Bi/AC. These were due to the high loading of Bi_2O_3 particles and the surfaces that possessed high mesopore structures ranging from 2 to 50 nm. Consequently, it had a correlation with resulting in the largest average pore diameter of 2.59 nm as compared to the other adsorbents. Furthermore, it was noticeable that S_{mic} (296.31 m^2/g) and micropore volume, V_{mic} (0.12 cm^3/g) for 0.5Bi/AC were significantly low, which explained that some of Bi_2O_3 particles were capable to enter and block the micropores of AC. The pores were mainly responsible for CO_2 adsorption as they provided enough spaces for the molecules to accommodate into the pores.

IR spectra of the adsorbents are described in Figure 5, whereas the absorption peaks are tabulated in Table 2. The absorption peaks at 1080 and 1302 cm^{-1} were assigned to CH_3 rocking mode $\rho(CH_3)$ [32] and C-O stretching for carboxyl, respectively. Other bands of carboxyl group were C=O asymmetry and O-H bend at 1640 and 1413 cm^{-1}, respectively. A sharp absorption band at 1560 cm^{-1} and a weak band at 2974 cm^{-1} corresponded to C=C aromatic and C-H stretching for alkyl, respectively. The very broad band

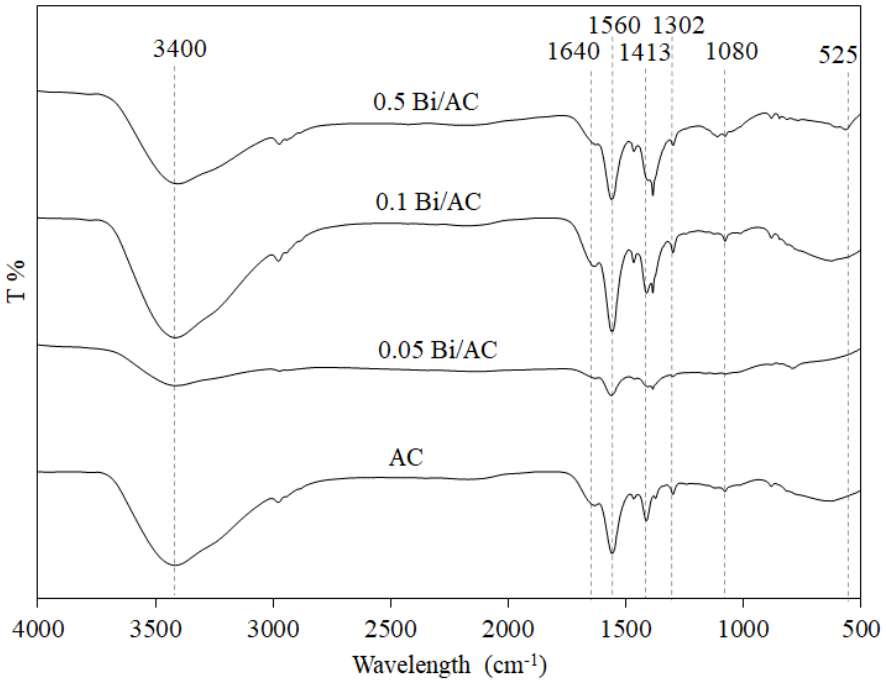

Figure 5. IR spectra of AC and Bi/ACs series

Table 2. IR frequencies and band assignments for adsorbents

Wavenumber (cm^{-1})	Band assignment	References
525	Bi-O	525
1080	CH_3 rocking mode ρ(CH_3)	1090
1302	C-O stretch for carboxyl	1210-1320
1413	OH bend for carboxyl	1395-1440
1560	Aromatic C=C	1560-1580
1640	C=O asymmetry for carboxyl	1540-1650
2974	C-H stretch (alkyl)	~3000
3700-3200	O-H stretch	3500-3200

at around 3500-3200 cm^{-1} was attributed to O-H stretch vibrational mode due to the adsorbed water molecules and carboxyl O-H stretching. The peaks in the range of 300-600 cm^{-1} showed the existence of metal-oxygen interactions [33]. 0.5Bi/AC exhibited an absorption peak at 525 cm^{-1} that was assigned to Bi-O stretching [34], which confirmed the presence of Bi_2O_3 in the AC composites.

Adsorption Capacity

The wide angle of the thermograms for CO_2 capture was plotted, as shown in Figure 6. Initial weight loss corresponded to moisture and humidity gas removal when exposed to the temperature of 350°C. The temperature was reduced to 30°C for CO_2 adsorption screening. The measurement was conducted for 20 minutes with its weight gain over the CO_2 exposure was important to determine the adsorption capacity. The reaction was followed by desorption process by switching gas feed to N_2 with thermal exposure up to 900°C.

Figure 7 shows the adsorption capacity over time, which a clear adsorption process can be observed. The adsorption and desorption capacities were calculated using equation (1).

$$Adsorption\ capacity\ (mg/g) = \frac{wt_{a.ads}(mg) - wt_{i.ads}\ (mg)}{wt_{i.ads}\ (g)} \quad (1)$$

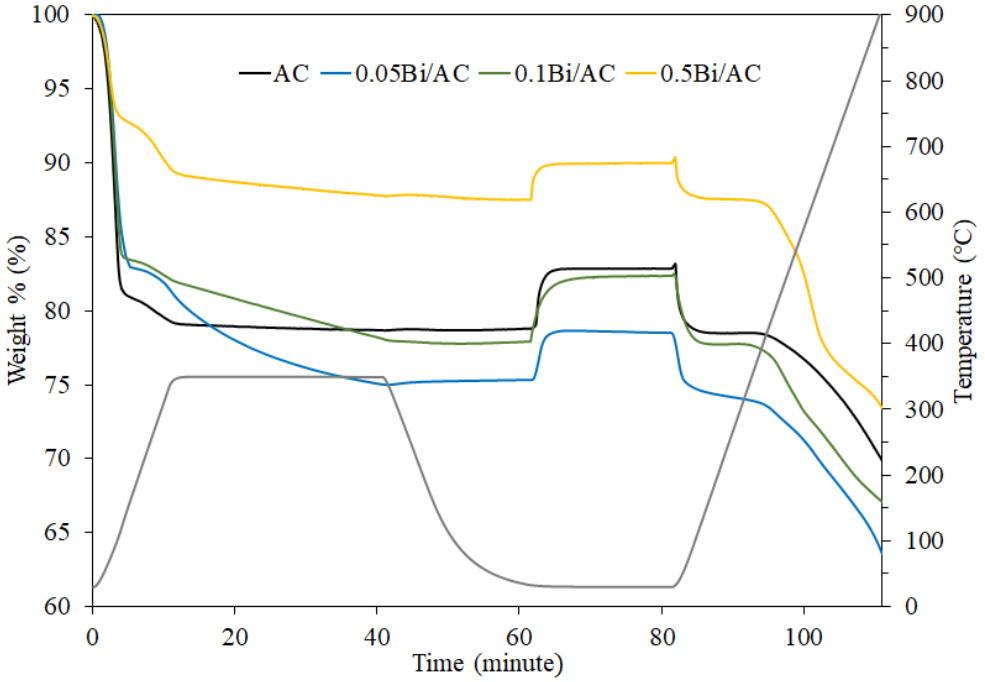

Figure 6. Wide angle thermograms for CO_2 capture at adsorption temperature of 30°C.

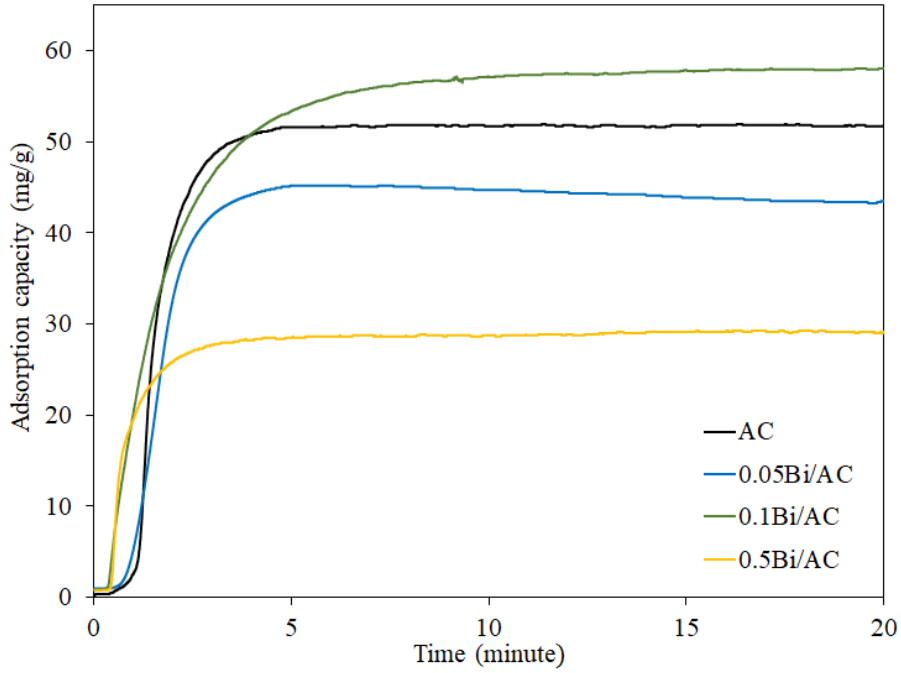

Figure 7. Adsorption capacity for 0.1Bi/AC by saturation purge of purified CO_2 gas

Where, $wt_{a,ads}$ (mg) is the weight after CO_2 adsorption, $wt_{i,ads}$ (mg) is the initial weight right before CO_2 adsorption. 0.1Bi/AC and 0.5Bi/AC had faster adsorption compared to 0.05Bi/AC and AC. It was due to the affinity of Bi_2O_3 to attract CO_2, which might formed CO_2-adsorbed products such as linear CO_2 and other carbonate species. It was found that 0.1Bi/AC was the most efficient adsorbent with an adsorption capacity of 58.71 mg/g. The highest Bi_2O_3 loading of 0.5Bi/AC showed the lowest adsorption capacity ascribed to the inefficient of agglomeration of Bi_2O_3 particles that reduced the responsible active sites of Bi_2O_3 and adsorption sites of AC.

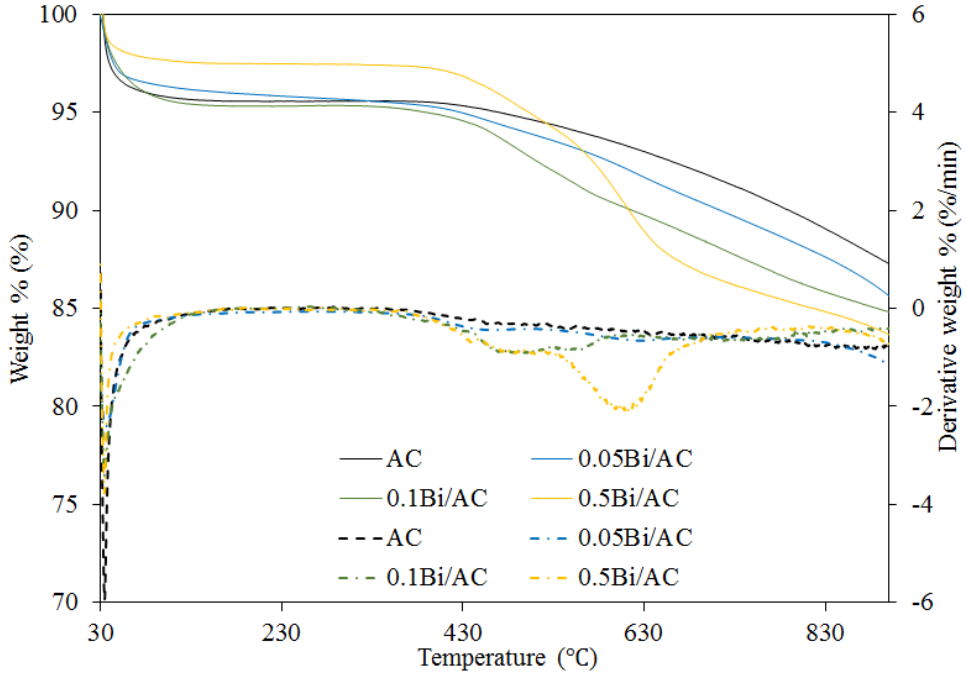

Figure 8. TGA-DTG analysis for the desorption process

TGA-DTG analysis (Figure 8) showed 0.5Bi/AC had low capability in CO_2 desorption by losing about 2.79% of weight at 400°C. The rest of the adsorbents showed about two times higher weight loss compared to 0.5Bi/AC. At 400 - 540°C, the desorption process may involved dissociation of chemically bonded carbonate species and removal of oxygen. A significant weight loss around 540 – 700°C for 0.5Bi/AC might be corresponded to polydentate carbonate species that commonly involved strong chemical bonds. After this temperature range, the metal oxide was regenerated but in a different chemical unit due to the removal of oxygen. Therefore, an efficient desorption temperature for recyclability test is 400°C because it does not involve any chemical formula unit and it is sufficient to regenerate adsorbed CO_2. For 0.05Bi/AC and 0.1Bi/AC, having highly dispersed Bi_2O_3 particles on AC resulted in efficient physisorption, chemisorption, and regeneration of CO_2. However, 0.1Bi/AC showed larger weight loss at 400 to 540°C than the other adsorbents. This indicated that 0.1 M loading concentration was efficient to be well dispersed on AC with the active and adsorption sites highly interacted with the probe molecules of CO_2. In addition, AC acquired a synergic effect on CO_2 adsorption upon Bi_2O_3 loading into its porous structure. There are two possible reasons for the synergic effect of AC, which are high surface area and uniform microporous surface of AC. When Bi_2O_3 was loaded onto AC, more CO_2 affinity sites were exposed to the adsorbate and thus the adsorption capacity increased [35].

Adsorption and desorption capacity values of the adsorbents were compared as shown in Figure 9. The desorption capacity was calculated from the weight loss of TGA analysis by using equation (2).

$$Desorption\ capacity\ (mg/g) = \frac{wt_{i.des}(mg) - wt_{a.des}\ (mg)}{wt_{a.ads}\ (g)} \quad (2)$$

Where, $wt_{i,des}$ (mg) is the initial weight as desorption begins and $wt_{a,des}$ (mg) is the weight after desorption. Discrepancies between the adsorption and desorption capacities might be due to traces of moisture adsorbed from the CO_2 gas feed during adsorption and volatile water molecules that strongly bonded which were unable to be desorbed during the cleaning process. The presence of traces of water content on metal oxide creates hydroxyl surface that generates bicarbonate species. Hence, the adsorption capacity for 0.05Bi/AC was affected by water molecules and formed high amounts of bicarbonate species. For 0.1Bi/AC, the Bi_2O_3 loading was sufficient with the presence of traces of water molecules to enhance CO_2 adsorption. Physically, the addition of Bi_2O_3 created uneven adsorbent surfaces that led to new morphology and heterogeneous surfaces. This structure can easily trap CO_2 through the voids by physisorption. Meanwhile, chemisorption occurred by affinity of Bi_2O_3 to attract CO_2.

The most efficient adsorbent, 0.1Bi/AC, was used to optimize the adsorption temperature, as shown in Figure 10. Adsorption temperatures of 40 and 50°C were found similarly significant in reducing adsorption capacity to about almost 2 times lower than 30°C. It is worth to mention that above 30°C, the adsorption mechanism was observed to be slightly

faster at the initial stage, which could be attributed to the heat supply that may activate reactions in generating carbonate species. Nevertheless, the heat supply may cause the species to be weakly bonded and physisorbed CO_2 molecules were easy to be removed once the adsorption has reached an equilibrium stage around after 4 minutes of adsorption. Hence, it can be concluded that 30°C is the optimum adsorption temperature for the adsorbent. Luevano-Hipolito et al. [27] have reported using Bi_2O_3 synthesized by sol-gel method at a lower temperature of 20°C, low pressure of 0.146 atm, and with the presence of water, and only attained a lower adsorption capacity of 42 mg/g. Whereas this work has synthesized Bi_2O_3/AC adsorbent using low Bi_2O_3 loading which measured higher adsorption capacity. Another work reported by Mendoza et al. [36] utilized extreme conditions of high pressure of 30 atm and 36 hours of adsorption time to obtain an adsorption capacity of 610.1 mg/g. Overall, this work presented a feasible reaction at ambient adsorption conditions with a comparable adsorption capacity.

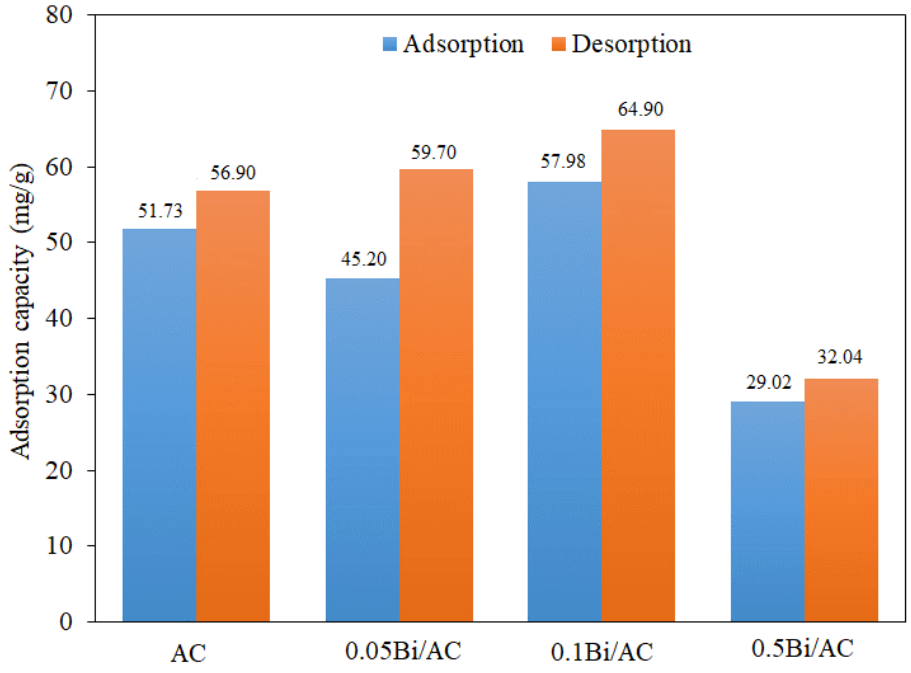

Figure 9. Comparison of CO_2 adsorption and desorption capacity values

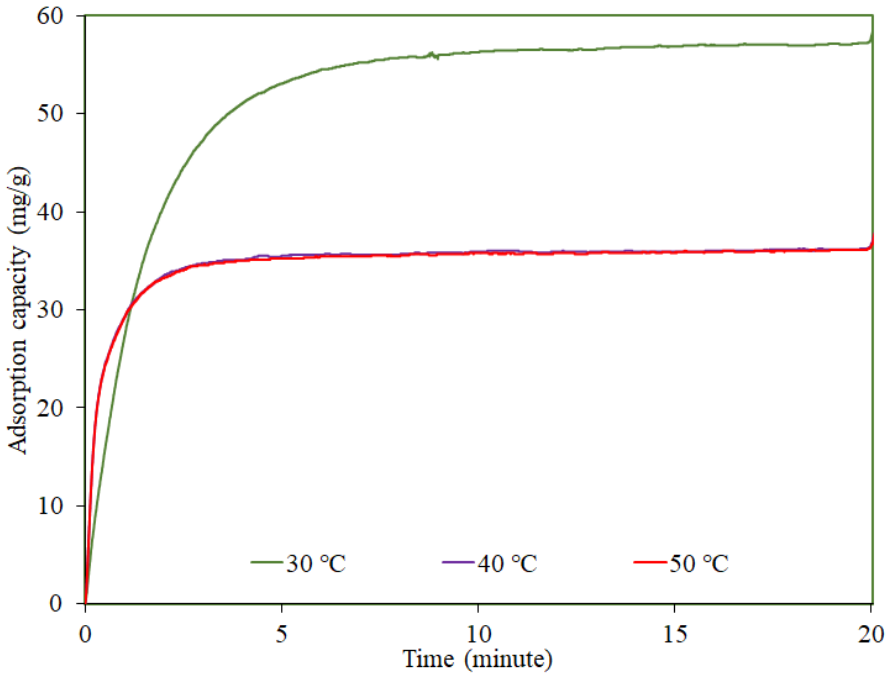

Figure 10. Adsorption capacity at different adsorption temperatures

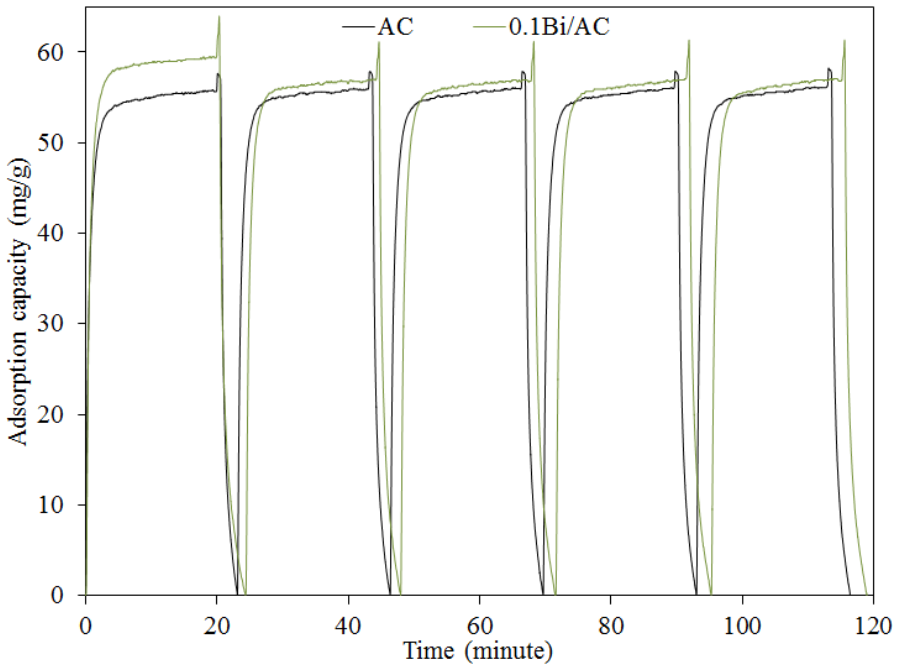

Figure 11. CO_2 capture recyclability with adsorption temperature at 30°C and desorption temperature at 400°C

Adsorption Kinetics

CO_2 capture stability performance for cyclical operation is important besides high selectivity and high adsorption capacity. The recyclability of CO_2 capture at adsorption temperature of 30°C and desorption temperature of 400°C for AC and 0.1Bi/AC is shown in Figure 11. Throughout the 5 cycles of CO_2 capture, no significant decline in adsorption capacity was observed. Although adsorption capacity of 0.1Bi/AC for the second cycle and above having slightly higher adsorption capacity compared to AC, the addition of Bi_2O_3 on AC was believed to have higher storage stability. This suggests that 0.1Bi/AC has a promising potential for further study towards practical applications.

Adsorption uptake rate can be established by using kinetic analysis. The Lagergren pseudo-first-order and pseudo-second-order kinetic models were performed for the effect of adsorption temperature on 0.1Bi/AC. Kinetic parameters at each temperature and its corresponding coefficient of determination are summarized in Table 3. The conformity of the experimental data and kinetics model was analysed by comparing the correlation coefficient (R^2) and calculated adsorption quantity ($q_{e.calc}$) with experimental adsorption quantity ($q_{e.exp}$) values. According to Demirbas et al. [37], the linearized Lagergren pseudo-first-order is expressed as in equation (3).

$$\log(q_e - q_t) = \log q_e - \left(\frac{k_1}{2.303}\right) t \qquad (3)$$

Based on Equation (3), q_t (mg/g) and q_e (mg/g) are the amounts of adsorbed at time t (minute) and the amount of the adsorbate adsorbed per unit weight of the adsorbents at equilibrium, respectively, and k_1 (min^{-1}) is the rate constant for pseudo-first-order rate expression. Pseudo-second-order kinetic model [38] is described in equation (4) below.

$$\frac{t}{q_t} = \frac{1}{k_2 q_e^2} + \left(\frac{1}{q_e}\right) t \qquad (4)$$

Where, k_2 (g/mg min) is the pseudo-second-order rate constant, t is the contact time in min, while q_e (mg/g) and q_t (mg/g) are the adsorption capacity at equilibrium and particular time, respectively.

The linearized plots of pseudo-first-order kinetic for log (q_e–q_t) against t at various adsorption temperatures are described in Figure 12. The slope and intercept of the plots of log (q_e-q_t) against t were used to calculate the values of k_1 and $q_{e.calc}$. An assumption of pseudo-first-order kinetic is the rate of adsorption is directly proportional to the number of available free active sites on the adsorbent surfaces. Based on the kinetic parameters, the low values of R^2 and the large deviation between $q_{e.calc}$ and $q_{e.exp}$ values, as in Table 3, indicated that the experimental data did not fit the pseudo-first-order kinetic model. Adsorption rate (minute) was observed to decrease with respect to temperature. It was due to the higher kinetic energy of CO_2 adsorbate at elevated temperature, which may cause in high tendency to escape from the adsorbent surfaces. Pseudo-second-order kinetic linearized plot of t/q_t versus t is shown in Figure 13. The values of the calculated adsorption capacity, q_t for various adsorption temperatures were close to the values of experimental adsorption capacity, q_e (Table 3). Furthermore, R_2 values were greater than 0.99,

resulting in a better fit with the pseudo-second-order kinetic model. Hence, CO_2 adsorption kinetics was in agreement with the pseudo-second-order kinetic, suggesting a chemisorption process [39]. This involved chemical ion exchange at the active sites and deposition on the adsorbent surfaces.

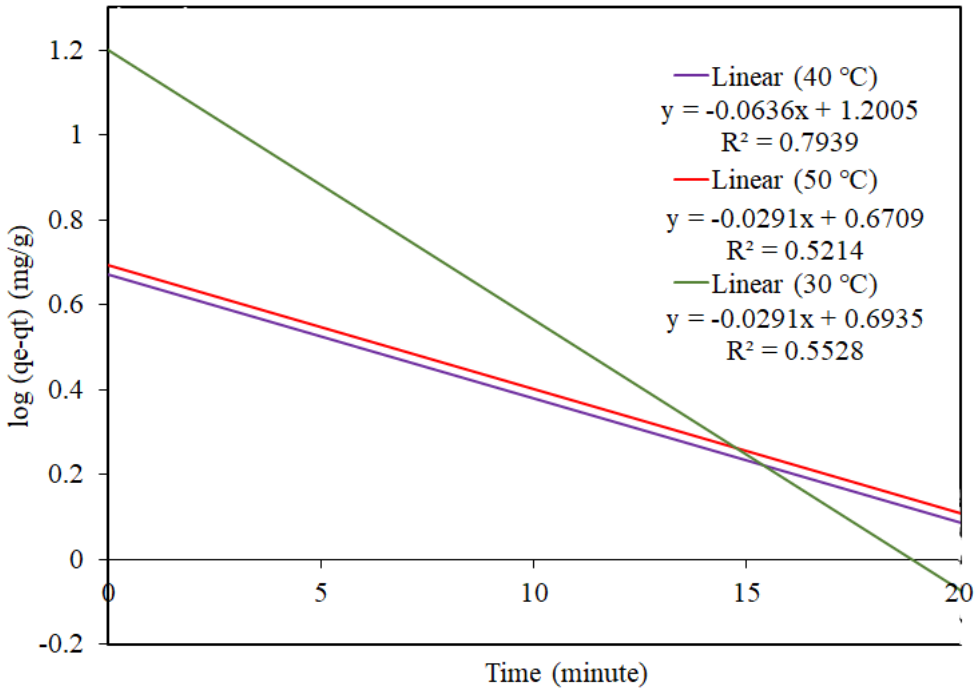

Figure 12. Linearized pseudo-first-order kinetic for 0.1Bi/AC at various adsorption temperatures

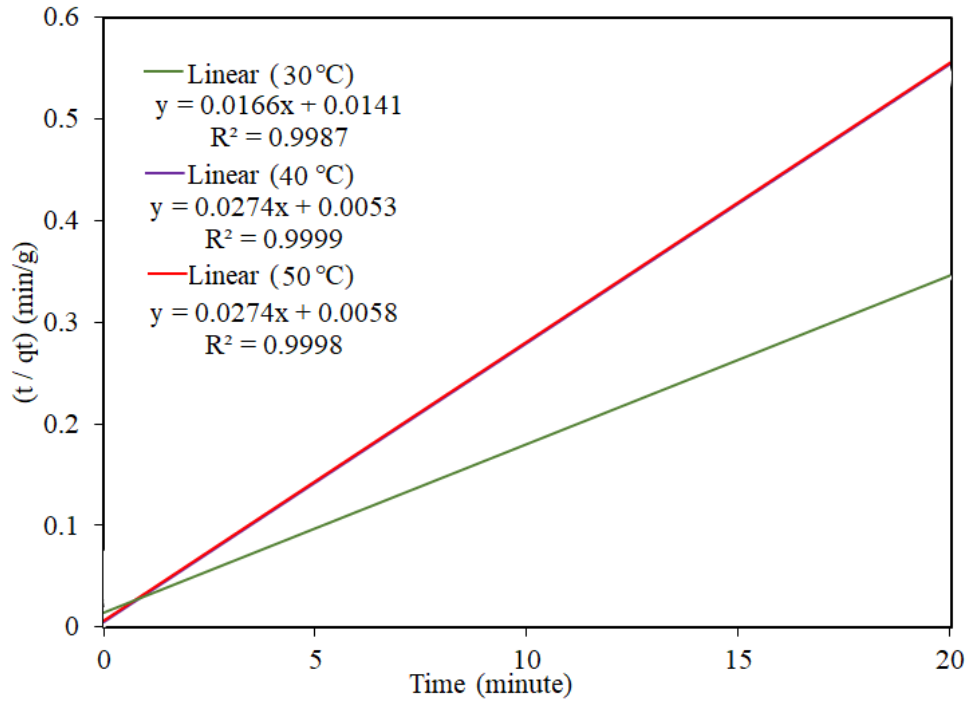

Figure 13. Linearized pseudo-second-order kinetic for 0.1Bi/AC at various adsorption temperatures

Table 3. The kinetic parameters for CO_2 adsorption at various adsorption temperatures

Model		Pseudo-first order kinetic $\log (q_e - q_t) = \log q_e - (k_1/2.303)t$			Pseudo-second order kinetic $t/q_t = 1/k_2.q_e^2 + t/q_e$		
Plot		$\log (q_e - q_t)$ vs. t			t/q_t vs. t		
Parameters	$q_{e,exp}$ (mg/g)	k_1 (1/min)	$q_{e,cal.}$ (mg/g)	R^2	k_2 (g/mg min)	$q_{e\ cal.}$ (mg/g)	R^2
30 °C	58.71	0.147	15.87	0.794	0.0141	60.24	0.999
40 °C	37.84	0.067	4.69	0.521	0.0141	36.50	0.999
50 °C	37.81	0.067	4.99	0.553	0.125	36.45	0.999

CONCLUSION

This study showed that 0.1Bi/AC was the most efficient adsorbent with adsorption capacity of 58.71 mg/g at the optimum adsorption temperature of 30°C. The recyclability test showed consistency after 5 cycles, which showed the potential for large scale applications. 0.1 M loading on AC gave a promising adsorption capacity with well-dispersed Bi_2O_3 on AC surfaces. The addition of Bi_2O_3 on AC surfaces resulted in slightly lower S_{BET} but enhanced the adsorption capacity by chemisorption; besides physisorption on the non-uniform adsorbent surfaces. SEM images for 0.1Bi/AC showed that surfaces were rougher and non-uniform, where only certain spots were brighter than usual that were caused by the immersion of Bi_2O_3 into AC and deposited on AC surfaces. The kinetic analysis of CO_2 adsorption onto 0.1Bi/AC was studied by using pseudo-first and pseudo-second-order kinetic models. The adsorption data at various adsorption temperatures showed the best fit with the pseudo-second-order kinetic model with R^2 = 0.99, indicating that chemisorption dominated the adsorption process and was the rate-controlling step.

ACKNOWLEDGEMENT

The authors are grateful to Department of Basic Science and Engineering, Universiti Putra Malaysia Kampus Bintulu and School of Chemical Sciences, Universiti Sains Malaysia for the research facilities, and Ministry of Higher Education for the financial support (Grant numbers: GP-IPM-9657200, GP-IPM-9559000, 1001.PKIMIA.811333, and 1001.PKIMIA. 822215).

REFERENCES

1. Shafeeyan, M. S., Wan Daud, W. M. A., Houshmand, A. and Shamiri, A. (2010) A review on surface modification of activated carbon for carbon dioxide adsorption. *Journal of Analytical and Applied Pyrolysis*, **89**,143-151.

2. Edenhofer, O, Pichs-Madruga, R and Sokona, Y. (2014) Climate change 2014 mitigation of climate change: working group III contribution to the fifth assessment report of the intergovernmental panel on climate change, Cambridge University Press. New York, USA.

3. Tan, Y. L., Islam, M. A., Asif, M. and Hameed, B. H. (2014) Adsorption of carbon dioxide by sodium hydroxide-modified granular coconut shell activated carbon in a fixed bed. *Energy*, **77,** 926-931.

4. Plaza, M. G., Pevida, C., Arias, B., Fermoso, J., Arenillas, A., Rubiera, F. and Pis, J. (2008) Application of thermogravimetric analysis to the evaluation of aminated solid sorbents for CO_2 capture. *Journal of Thermal Analysis and Calorimetry*, **92,** 601-606.

5. Tans, P. and Keeling, R. (2019) Trends in atmospheric carbon dioxide. National. Earth System Research Laboratory Global Monitoring Division, National Oceanic and Atmospheric Administration (NOAA). U. S. Department of Commerce.

6. Hakim, A., Abu Tahari, M. N., Mazrliza T. S., Wan Ishak, W. N. R., Yusop, M. R., Mohamed Hisham, M. W. and Yarmo, M. A. (2015) Study of CO_2 adsorption and desorption on activated carbon supported iron oxide by temperature programmed desorption. *Jurnal Teknologi (Sciences & Engineering)*, **77,** 75-84.

7. Chanapattharapol, K. C., Krachuamram, S. and Youngme, S. (2017) Study of CO_2 adsorption on iron oxide doped MCM-41. *Microporous and Mesoporous Materials*, **245,** 8-15.

8. Corti, A., Fiaschi, D. and Lombardi, L. (2004) Carbon dioxide removal in power generation using membrane technology, *Energy*, **29,** 2025-2043.

9. Rashidi, N. A., Yusup, S. and Hameed B. H. (2013) Kinetic studies on carbon dioxide capture using lignocellulosic based activated carbon, *Energy*, **61,** 440-446.

10. Akanksha, K. K. P. and Srivastava, V. K. (2007) Carbon dioxide absorption into monoethanolamine in a continuous film contactor, *Chemical Engineering Journal*, **133,** 229-237.

11. An, H., Feng, B. and Su, S. (2011) CO_2 capture by electrothermal swing adsorption with activated carbon fibre materials, *International Journal of Greenhouse Gas Control*, **5,** 16-25.

12. Luis, P., Gerven, T. V. and Bruggen, B. V. (2012) Recent developments in membrane-based technologies for CO_2 capture, *Progress in Energy and Combustion Science*, **38,** 419-448.

13. Zhang, Z., Xu, M., Wang, H. and Li, Z. (2010) Enhancement of CO_2 adsorption on high surface area activated carbon modified by N_2, H_2 and ammonia, *Chemical Engineering Journal*, **160,** 571-577.

14. Hakim, A., Marliza, T. S., Abu Tahari, N. M., Wan Isahak, R. W. N., Yusop, R. M., Mohamed Hisham, M. M and Yarmo, A. M. (2016) Studies on CO_2 adsorption and desorption properties from various types of iron oxides (FeO, Fe_2O_3, and Fe_3O_4), *Industrial & Engineering Chemistry Research*, **55,** 7888-7897.

15. Rosynek, M. P. and Magnuson, D. T. (1977) Infrared study of CO_2 adsorption on lanthanum sesquioxide and trihydroxide, *Journal of Catalysis*, **48,** 417-421.

16. Okawa, Y. and Tanaka, K. (1995) STM investigation of the reaction of Ag-O added rows with CO_2 on a Ag(1 1 0) surface, *Surface Science*, **344,** 1207-1212.

17. Takahashi, H., Yuki, K. and Nitta, T. (2002) Chemical modification of rutile TiO_2 (1 1 0) surface by ab initio calculations for the purpose of CO_2 adsorption, *Fluid Phase Equilibria*, **194,** 153-160.

18. Wan Isahak, W. N. R., Che Ramli, Z. A., Ismail, M. W., Ismail, K., Yusop, R. M., Mohamed Hisham, M. W. and Yarmo, M. A. (2013) Adsorption−desorption of CO_2 on different type of copper oxides surfaces: physical and chemical attractions studies, *Journal of CO_2 Utilization*, **2,** 8-15.

19. Hess, G., Froitzheim, H. and Baumgartner, C. (1995) The adsorption and catalytic decomposition of CO_2 on Fe(111) surfaces studied with high resolution EELS, *Surface Science*, **14,** 331-333.

20. Yoshikawa, K., Sato, H., Kaneeda, M. and Kondo, J. N. (2014) Synthesis and analysis of CO_2 adsorbents based on cerium oxide, *Journal of CO_2 Utilization*, **8,** 34-38.

21. Bagherisereshki, E., Tran, J., Lei, F. Q. and AuYeung, N. (2018) Investigation into SrO-$SrCO_3$ for high temperature thermochemical energy storage, *Solar Energy*, **160,** 85-93.

22. Hakim, A., Wan Isahak, W. N. R., Abu Tahari, M. N., Yusop, M. R., Mohamed Hisham, M. W. and Yarmo, M. A. (2014) Temperature programmed desorption of carbon dioxide for activated carbon supported nickel oxide: the adsorption and desorption studies, *Advanced Materials Research*, **1087,** 45-49.

23. Ma, W.,Wang, N., Lu., Lu, Z. Y., Tang, X. and Li, S. T. (2019) Synthetic of magnetic biomass carbon-based Bi_2O_3 photocatalyst and mechanism insight by a facile microwave and deposition method, New Journal of Chemistry, **43,** 2888-2898.

24. Karnan, T., Selvakumar, S. A. S., Adinaveen, T. and Suresh, J. (2016) Visible light induced photocatalytic degradation of azo dye by Bi_2O_3 nanoparticles synthesized using greener route, *International Journal of Scientific & Engineering Research*, **7,** 266-270.

25. Ayekoe, P. Y., Robert, D. and Gone, D. L. (2018) Facile synthesis of TiO_2/Bi_2O_3 heterojunctions for the photocatalytic degradation of water contaminants, *Journal of Materials and Environmental Sciences*, **9,** 2247-2253.

26. Sparks, D. E., Patterson, P. M., Jacobs, G., Dogimont, N., ,Tackett, A. and Crocker, M. (2006) Bi_2O_3/Al_2O_3 catalysts for the selective reduction of NO with hydrocarbons in lean conditions, *Applied Catalysis B: Environmental*, **65,** 44-54.

27. Luevano-Hipolito, E., Torrez-Martinez, L. M., Triana, C. and Lee, S. W. (2019) Ink-jet Bi_2O_3 films and powders for CO_2 capture and self-cleaning applications, *Thin Solid Films*, **677,** 83-89.

28. Shah, I., Adnan, R., Wan Ngah, W. S. and Mohamed, N. (2015) Iron impregnated activated carbon as an efficient adsorbent for the removal of methylene blue: regeneration and kinetics studies, *PLoS ONE*, **10,** 1-23.

29. Klinkova, L. A., Nikolaichik, V. I., Barkovskii, N. V., Fedotov, V. K. (2007) Thermal stability of

Bi_2O_3, *Russian Journal of Inorganic Chemistry*, **52,** 1822-1829.

30. Sing, K. S. W., Everett, D. H., Haul, R. A. W., Moscou, L., Pierotti, R. A. and Rouquerol, J. (1985) Reporting physisorption data for gas/solid systems with special reference to the determination of surface area and porosity, *Pure & Applied Chemistry*, **57,** 603-619.

31. Condon, J. B. (2006) Surface area and porosity determinations by physisorption measurements and theory, first ed., Elsevier, Netherland.

32. Inel, G. A., Ungureau, E. M., Varley, T. S., Hirani, M. and Holt, K. B. (2016) Solvent–surface interactions between nanodiamond and ethanol studied with in situ infrared spectroscopy, *Diamond & Related Materials*, **61,** 7-13.

33. Joo, S. H., Pak, C., You, D. J., Lee, H. I., Kim, J. M. and Seung, D. (2006) Ordered mesoporous carbons (OMC) as supports of electrocatalysts for direct methanol fuels (DMFC), *Electrochimica Acta*, **52,** 1618-1626.

34. Thirumurthy, K. and Thirunarayanan, G. (2018) A facile designed highly moderate craspedia flowerlike sulphated Bi_2O_3-fly ash catalyst: Green synthetic strategy for (6*H*-pyrido[3,2- b] carbazol-4-yl) aniline derivatives in water, *Arabian Journal of Chemistry*, **11,** 443-452.

35. Xu, X., Song, C., M. Andresen, J., G. Miller, B. and W. Scaroni, A. (2002) Novel polyethylenimine-modified mesoporous molecular sieve of MCM-41 type as high-capacity adsorbent for CO_2 Capture, *Energy & Fuels*, **16,** 1463-1469.

36. Demirbas, E., Kobya M., Senturk, E. and Ozkana, T. (2004) Adsorption kinetics for the removal of chromium (VI) from aqueous solutions on the activated carbons prepared from agricultural wastes, *Water SA*, **30**, 533-559.

37. Mendoza, E. Y. M., Santos, A. S., Lopez, E. V., Drozd, V., Durygin, A., Chen, J. H. and Saxena, S. K. (2019) Iron oxides as effiecient sorbents for CO_2 capture, *Journal of Materials Research and Technology*, **8,** 2944-2956.

38. Ho, Y.S., Mckay, G., Wase, D. & Foster, C.F. (2000) Study of the sorption of divalent metal ions on to peat, *Adsorption Science & Technolology,* **18,** 639-650.

39. Riahi, K., Chaabane, S. and Thayer, B. B. (2017) A kinetic modeling study of phosphate adsorption onto *Phoenix dactylifera* L. date palm fibers in batch mode, *Journal of Saudi Chemical Society*, **21,** S143-S152.